ELSEVIER

Chemical Physics 279 (2002) 143–159

Chemical Physics

www.elsevier.com/locate/chemphys

Density functional study of the vibrational frequencies of Lindqvist polyanions

Adam J. Bridgeman[a,*], G. Cavigliasso[a,b]

[a] *Department of Chemistry, University of Hull, Kingston-upon-Hull, HU6 7RX Hull, UK*
[b] *Department of Chemistry, University of Cambridge, Lensfield Road, Cambridge, CB2 1EW UK*

Received 17 January 2002

Abstract

The structures and vibrational spectra of the Lindqvist polyanions $[Mo_6O_{19}]^{2-}$, $[W_6O_{19}]^{2-}$, $[Mo_6O_{19}]^{3-}$, $[VMo_5O_{19}]^{3-}$ and $[VMo_5O_{19}]^{4-}$ have been calculated using density functional theory. The agreement between the previously reported vibrational spectra and the calculated values is extremely good. For $[Mo_6O_{19}]^{2-}$, a detailed comparison between the performance of commonly used functionals and basis sets and between Hartree–Fock and density functional methods has been performed. Whilst all density functional methods perform adequately, the Hartree–Fock method overestimates the strength of the metal–oxygen bonding and this is reflected in poor reproduction of the stretching frequencies. The results suggest that the local density approximation with Slater type orbitals and relativistic corrections is best able to model both the structure and vibrational spectra of these polyanions when treated as pseudo-gas phase species. The calculations are extremely computationally demanding requiring precise energies and geometries and cannot presently be considered a standard task for the study of these large, heavy element cluster anions. The vibrational analyses confirm the high symmetry for these anions suggested by previous geometry calculations.

1. Introduction

The polyoxometalates form an extremely large and diverse group of compounds with remarkable chemical and physical properties [1,2]. Polyoxometalates are used and have potential applications in a variety of fields including medicine, catalysis, solid-state technology and chemical analysis [3,4]. The polymerization of oxoanions to form extended metal–oxygen cluster anions is largely restricted to vanadium, niobium, tantalum, molybdenum and tungsten. These polyanions are built primarily by edge and, occasionally, corner sharing of MO_6 octahedra and the resulting cages are usually approximately spherical. The $[M_6O_{19}]^{n-}$ isopolyanions are an important illustrative class. The Lindqvist structure of these anions, shown in Fig. 1, is a compact assemblage of edge-sharing octahedra leading to an overall octahedral cluster. Unlike many of the other structural types, the hexametalate structure is adopted

* Corresponding author.
E-mail address: a.j.bridgeman@hull.ac.uk (A.J. Bridgeman).

0301-0104/02/$ - see front matter
PII: S0301-0104(02)00450-0

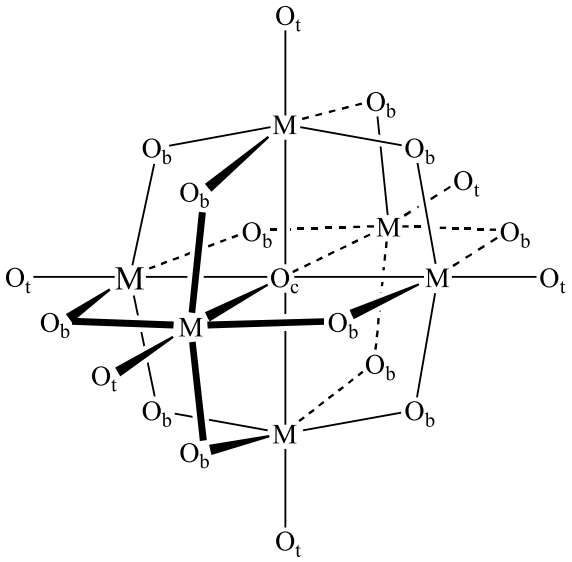

Fig. 1. Structure of Lindqvist polyanions showing the labelling of terminal (t), bridging (b) and central (c) oxygen atoms.

by the full range of 4d and 5d polyanion forming metal ions (Nb^{V}, Ta^{V}, Mo^{VI} and W^{VI}). All of these anions have structures which are close to the ideal O_h symmetry, $[Nb_6O_{19}]^{8-}$ [5], $[Ta_6O_{19}]^{8-}$ [6], $[Mo_6O_{19}]^{2-}$ [7] and $[W_6O_{19}]^{2-}$ [8]. The available structural information for these anions has been reviewed and compiled by Tytko et al. [9]. In addition, hexametalate clusters containing a mixture of Group 5 and Group 6 metal ions have been isolated and studied spectroscopically [10–12]. No direct structural information for these mixed metal anions appear to have been reported due to the problem of disorder in the crystallographic characterization. Each metal in the Lindqvist structure is strongly bonded to one terminal oxygen atom leading to a categorization of Type I in Pope's classification scheme [1]. Type I systems undergo reversible redox reduction with minor structural changes. Electron spin resonance (ESR) and ^{17}O nuclear magnetic resonance (NMR) have been used to probe the structure and possible mixed-valence character of the reduced $[Mo_6O_{19}]^{3-}$ anions. The ESR studies [13] indicate that the unpaired electron occupies a non-degenerate orbital with limited ground state delocalization restricted to ligand oxygen atoms. The NMR results [14], however, suggest that the additional electron is delocalized over all the metal atoms and that the anion maintains effective cubic symmetry, at least on the NMR timescale.

In addition to the crystallographic, ESR and NMR studies of the hexametalates, vibrational spectroscopy has been used to investigate the structure and bonding. However, the assignment of IR and Raman spectra of such clusters is problematic and complicated. A number of normal coordinate analyses of hexametalate polyanions using the semi-empirical Wilson GF method [15] have been reported utilizing internal coordinate basis sets at varying levels of sophistication. An octahedral $[M_6O_{19}]^{n-}$ ion has 69 normal modes of which 7 are infrared-active and 11 Raman-active fundamentals. The infrared (IR) and Raman spectra and normal coordinate analyses of $[Nb_6O_{19}]^{8-}$ and $[Ta_6O_{19}]^{8-}$ have been reported by von Mattes et al. [16] and Farrel et al. [17]. The vibrational spectra of the $[Mo_6O_{19}]^{2-}$ and $[W_6O_{19}]^{2-}$ ions have also been studied by von Mattes et al. The most detailed normal coordinate analyses have been reported by Rocchiccioli-Deltcheff and co-workers [18,19] for the $[Mo_6O_{19}]^{2-}$, $[Mo_6O_{19}]^{3-}$ and $[VMo_5O_{19}]^{3-}$ ions using 162 internal coordinates. The IR and Raman spectra of these ions and of the reduced $[VMo_5O_{19}]^{4-}$ ion have also been reported by Buckley and Clark [12]. The assignment of the spectra and the calculation of the force field is made difficult by both the large number of internal coordinates and the high symmetry of the anions which leads to relatively few IR and Raman active modes, not all of which are actually apparent in the spectra. No non-empirical computational study of the vibrational spectra of the hexametalates has, to the best of our knowledge, been reported.

Although the synthesis, structural and spectroscopic analysis and development of applications of polyoxoanions are extremely rich areas of research, relatively few high-level computational studies have been reported – reflecting the intensive computational demands imposed by the large size of these species. Most of the first-principle studies related to polyanions have been carried out by Poblet, Bénard and co-workers [20–30], at the Hartree–Fock (HF) and density functional (DF)

levels of theory, and by Bridgeman and Cavigliasso [31–35], and Borshch and co-workers [36–38] at the DF level.

We have recently published a detailed analysis of the structure and bonding in $[M_6O_{19}]^{n-}$ isopolyanions of Nb, Ta, Mo and W [35]. In this paper, we extend this study by reporting the first non-empirical computational study of the vibrational spectra of $[Mo_6O_{19}]^{2-}$, $[W_6O_{19}]^{2-}$, $[Mo_6O_{19}]^{3-}$, $[VMo_5O_{19}]^{3-}$ and $[VMo_5O_{19}]^{4-}$ to assist the assignment of the experimental results. Such a vibrational analysis is extremely computationally demanding and we report a comparison of the results obtained using a number of the most widely used basis sets and density functionals.

2. Computational approach

Density functional (DF) calculations have been performed with the ADF [39,40] and Gaussian 98 [41] programs. Hartree–Fock (HF) calculations have been performed with Gaussian 98 [41]. The ADF program uses Slater type orbital (STO) basis sets. Previous studies [31–35] indicate that an STO basis set of triple-ζ quality incorporating frozen cores and the ZORA relativistic approach [39,40] (ADF Type IV basis set) on all atoms yields good results on polyanions. This basis set (labelled as **A** below) was used in all ADF calculations. Gaussian 98 uses Gaussian type orbital (GTO) basis sets. Calculations were performed with the widely used LANL2DZ and SDD GTO basis sets (labelled **B** and **C** below). These use quasi-relativistic effective core potentials to represent the atomic cores and are of double and triple-ζ quality, respectively.

The ADF program uses numerical differentiation of analytic first derivatives of the energy to obtain vibrational frequencies whilst the Gaussian 98 program uses analytical second derivatives. Accurate numerical differentiation requires precise numerical integration and self-consistent field (SCF) convergence for the energy. Initial calculations using the default integration and SCF convergence criteria for vibrational frequencies in the ADF program lead to the prediction of imaginary frequencies for symmetry lowering vibrational modes for a number of the systems. These imaginary frequencies were removed by increasing the integration and convergence criteria (to 10^{-7} and 10^{-6}, respectively). The calculation of vibrational frequencies using this method is a demanding task for these large anions. For example, an unrestricted, gradient corrected calculation of the geometry of the C_{4v} $[Mo_6O_{19}]^{3-}$ anions required around 6 h on a 1 GHz Pentium IV machine whilst the subsequent calculation of the frequencies took over four weeks! Nevertheless, there is evidence, on related systems, that frequencies calculated using this approach may be slightly better than those calculated using GTO basis sets of comparable size [42,43].

Calculations of the structure and vibrational frequencies of the $[Mo_6O_{19}]^{2-}$ ion were performed using these sets of basis orbitals and a variety of functionals. Functionals based on the Vosko–Wilk–Nusair (labelled VWN) form [44] of the local density approximation (LDA), on a combination of Becke's 1988 exchange [45] and Perdew's 1986 correlation [46] corrections (labelled BP86) and on a combination of Becke's 1988 exchange and the Lee–Yang–Parr correlation [47] correction (labelled BLYP) were used for each basis set. In addition, calculations were performed with the GTO basis sets using Becke's three parameter hybrid functional B3LYP [48]. Hybrid functionals are not available in the ADF program. For comparison, calculations of the structure and vibrational frequencies of $[Mo_6O_{19}]^{2-}$ were also performed at the HF level with basis sets **B** and **C**.

Geometry optimizations and calculation of vibrational frequencies were also performed for the $[Mo_6O_{19}]^{3-}$, $[W_6O_{19}]^{2-}$, $[VMo_6O_{19}]^{3-}$ and $[VMo_6O_{19}]^{4-}$. Our earlier calculations [35] on the $[Mo_6O_{19}]^{3-}$ ion indicate that the unpaired electron resides in an orbital derived from an e_u function of the oxidized octahedral anion. This occupation leads to a small Jahn-Teller distortion towards a C_{4v} structure and either a $^2A_2$ or a $^2B_2$ state corresponding to a slight tetragonal elongation or compression respectively of the octahedral cage. Calculations have been performed for both states.

To be consistent with the majority of the earlier workers on these anions, the numbering system used for the vibrational modes below follows the character tables of Herzberg [49].

3. Results

3.1. Structure of the $[Mo_6O_{19}]^{2-}$ anion

Table 1 lists optimized Mo–O bond lengths for the $[Mo_6O_{19}]^{2-}$ anion using the atom labelling shown in Fig. 1. As discussed in more detail below, the vibrational analyses confirm that this anion has O_h symmetry in the gas phase as previously reported [35]. There is good agreement with the experimental results for the Mo–O_b bond lengths for all basis sets and functional combinations. The agreement for the central Mo–O_c and terminal Mo–O_t bonds is much more variable, however, with all calculations overestimating the bond lengths.

Although the anion has only a relatively small charge, delocalized over a fairly large cluster, it is probable that the neglect of crystal field stabilization in the isolated molecule calculations reported here is responsible for the poorer prediction of the bond length of the exposed Mo–O_t bonds. The best overall agreement is found for the STO/ZORA approach, consistent with previous reports [31]. The shortest Mo–O_t bond length is predicted at the LDA level using this approach. It appears that the well-known overbinding character of LDA functionals compensates for the deficiency of the isolated molecule calculations as previously reported [50,51]. For the GTO calculations, the bond lengths predicted using the LANL2DZ basis set are similar but appear to be slightly shorter than those predicted using the SDD basis set. The B3LYP approach improves agreement with the experimental bond lengths compared to the gradient corrected functionals. The BP86 bond lengths are shorter than those obtained using the BLYP gradient corrections for both GTO and STO basis sets. Thus, from a pragmatic point of view, at least, the STO/ZORA approach at the LDA level appears to be the best able to reproduce crystallographically determined geometries for these isopolyanions.

The geometries predicted using HF theory are comparable to those obtained at the LDA and the Mo–O_t bond lengths are actually closer to the experimental distances than those obtained by the various DF levels. The performance of basis sets **B** and **C** is again very similar. It appears the overbinding produced by the absence of correlation in the HF calculations compensates for the lack of crystal field. The ability of the HF method to accurately predict the geometry of polyanions has been previously discussed by Maestre et al. [25] for $[W_6O_{19}]^{2-}$ and was ascribed to the small role of correlation for the formally d^0 metal ions. However, the calculated charge of the metal ion in these anions correspond to d^3–d^4 configurations [31–35] and the apparent accuracy of the HF geometries is almost certainly due to a cancellation of errors. As

Table 1
Calculated and experimental [9] Mo–O bond distances for $[Mo_6O_{19}]^{2-}$

Computational method		Bond length (Å)		
Functional	Basis set	Mo–O_c	Mo–O_b	Mo–O_t
VWN	**A** [35]	2.32	1.93	1.71
	B	2.35	1.93	1.73
	C	2.41	1.97	1.76
BP86	**A**	2.36	1.96	1.73
	B	2.39	1.96	1.75
	C	2.39	1.96	1.74
BLYP	**A**	2.38	1.97	1.74
	B	2.41	1.97	1.76
	C	2.41	1.97	1.76
B3LYP	**B**	2.38	1.95	1.73
	C	2.39	1.95	1.73
HF	**B**	2.37	1.91	1.68
	C	2.37	1.92	1.68
	Experimental	2.32	1.92	1.68

discussed below, the HF method is unsuitable for the vibrational analysis of these ions.

3.2. Vibrational spectrum of the $[Mo_6O_{19}]^{2-}$ anion

As outlined in Section 1, the $[Mo_6O_{19}]^{2-}$ anion has 69 normal modes of vibration. For octahedral symmetry, these span:

$$\Gamma_{vib} = 3a_{1g}(R) + a_{2g} + 4e_g(R) + 3t_{1g} + 4t_{2g}(R) + a_{2u} + e_u + 7t_{1u}(IR) + 4t_{2u}$$

where the IR and Raman (R) activities are shown in parenthesis. Of the seven IR active bands, six were observed by Rocchiccioli-Deltcheff et al. [18]. Seven of the 11 Raman active bands were observed by these workers and a further three bands were reported by Buckley and Clark [12]. The three a_{1g} modes, however, were unambiguously identified from the polarized bands. Rocchiccioli-Deltcheff et al. also reported a normal coordinate analysis using 162 internal coordinates using isotopic substitution to assist the assignment and calculation of the force field.

Tables 2–6 list the calculated vibrational frequencies and assignments for all of the modes of the $[Mo_6O_{19}]^{2-}$ anion using the DF and HF methods and structures discussed above. Table 2 includes an approximate description of the modes in terms of the stretching (ν) and bending (δ) of the

Table 2
Calculated and experimental vibrational frequencies (in cm^{-1}) and assignments for $[Mo_6O_{19}]^{2-}$ at the VWN level

Mode		Experimental			Basis set			Approximate description
		[12]	[16]	[18]	**A**	**B**	**C**	
a_{1g}	ν_1	987	980	986	993	991	995	ν_s (Mo–O_t)
e_g	ν_6	954	951	958	963	963	967	ν_{as} (Mo–O_t)
t_{1u}	ν_{14}		957	956	962	963	967	ν_{as} (Mo–O_t)
e_g	ν_7	810	809	817	806	821	822	ν_{as} (Mo–O_b)
t_{1u}	ν_{15}		798	796	799	821	820	ν_{as} (Mo–O_b)
t_{2g}	ν_{21}				585	581	578	δ (O_b–Mo–O_t)
t_{1u}	ν_{16}		602	598	576	580	579	δ (O_b–Mo–O_t)
a_{1g}	ν_2	597	580	598	546	534	531	δ (O_b–Mo–O_t)
t_{2u}	ν_{25}				530	550	552	δ (O_b–Mo–O_t) + ν_{as} (Mo–O_b)
t_{2u}	ν_{26}				508	510	541	δ (O_b–Mo–O_t) + ν_{as} (Mo–O_b)
t_{1g}	ν_{11}				507	534	510	δ (O_b–Mo–O_t) + ν_{as} (Mo–O_b)
a_{2g}	ν_4				490	506	516	δ (O_b–Mo–O_t) + ν_{as} (Mo–O_b)
e_g	ν_8	440			481	478	475	δ (O_b–Mo–O_t) + ν_{as} (Mo–O_b)
t_{1u}	ν_{17}		438	432	447	457	458	δ (O_b–Mo–O_t)
a_{2u}	ν_5				442	464	471	δ (O_b–Mo–O_b)
t_{2g}	ν_{22}	329			416	436	441	δ (O_b–Mo–O_b) + ν_{as} (Mo–O_b)
t_{1u}	ν_{18}		356	352	358	387	385	ν_{as} (Mo–O_c)
a_{1g}	ν_3	286	278	285	289	290	289	ν_s (Mo–O_b)
e_u	ν_{10}				272	283	287	δ (O_b–Mo–O_b)
t_{1g}	ν_{12}				222	223	225	δ (O_b–Mo–O_t)
t_{2g}	ν_{23}	200	163	205	220	219	222	δ (Mo–O_b–Mo) + ν (Mo–O_b)
t_{1u}	ν_{19}		220	217	210	217	215	ν_{as} (Mo–O_b)
t_{1u}	ν_{20}		192		199	196	198	δ (O_b–Mo–O_b)
t_{2u}	ν_{27}				196	193	199	δ (O_b–Mo–O_b) + ν_{as} (Mo–O_b)
t_{2g}	ν_{24}	166	125	166	195	190	191	ν_{as} (Mo–O_b)
e_g	ν_9	207	197		154	157	158	ν_{as} (Mo–O_b)
t_{2u}	ν_{28}				134	140	142	ν_{as} (Mo–O_b)
t_{1g}	ν_{13}				77	118	133	δ (O_b–Mo–O_b)
RMS error assignment 1					19	24	25	
RMS error assignment 2					17	24	25	

The RMS error is calculated with respect to the data from [18].

Table 3
Calculated and experimental vibrational frequencies (in cm^{-1}) and assignments for $[Mo_6O_{19}]^{2-}$ at the BP86 level

Mode		Experimental			Basis set		
		[12]	[16]	[18]	**A**	**B**	**C**
a_{1g}	ν_1	987	980	986	957	954	955
e_g	ν_6	954	951	958	927	926	927
t_{1u}	ν_{14}		957	956	926	925	927
e_g	ν_7	810	809	817	757	765	768
t_{1u}	ν_{15}		798	796	750	763	764
t_{2g}	ν_{21}				555	545	544
t_{1u}	ν_{16}		602	598	550	551	551
a_{1g}	ν_2	597	580	598	521	508	508
t_{2u}	ν_{25}				502	501	500
t_{2u}	ν_{26}				457	464	469
t_{1g}	ν_{11}				462	478	486
a_{2g}	ν_4				432	439	451
e_g	ν_8	440			461	451	451
t_{1u}	ν_{17}		438	432	429	435	435
a_{2u}	ν_5				439	454	461
t_{2g}	ν_{22}	329			412	426	431
t_{1u}	ν_{18}		356	352	347	372	370
a_{1g}	ν_3	286	278	285	279	281	280
e_u	ν_{10}				267	276	279
t_{1g}	ν_{12}				221	217	219
t_{2g}	ν_{23}	200	163	205	217	215	219
t_{1u}	ν_{19}		220	217	206	207	206
t_{1u}	ν_{20}		192		190	191	194
t_{2u}	ν_{27}				191	184	190
t_{2g}	ν_{24}	166	125	166	193	187	189
e_g	ν_9	207	197		148	151	152
t_{2u}	ν_{28}				127	130	134
t_{1g}	ν_{13}				66	40	82
RMS error assignment 1					37	37	37
RMS error assignment 2					36	37	36

The RMS error is calculated with respect to the data from [18].

bonds. The assignment of modes to localized motions of atoms is only meaningful for the highest frequency (>900 cm^{-1}) vibrations which are predominately Mo–O_t stretches. The remainder of the vibrations involve fairly complex motions of many atoms and the separation into stretching and bending components for the Mo–O_b and Mo–O_c connections is difficult. Also included in the tables are the experimental frequencies and assignments due to Rocchiccioli-Deltcheff et al. [18], von Mattes et al. [16] and Buckley and Clark [12] which differ somewhat. The computational results are compared to the values reported by Rocchiccioli-Deltcheff et al. using the root mean square (RMS) error. These workers recorded both IR and Raman spectra at the same temperature.

The RMS error for assignment 1 is based on the assignments of Rocchiccioli-Deltcheff et al. The RMS error for this assignment in each case arises primarily from two modes. The three lowest frequency modes in the Raman spectrum appear at ca. 166, 200 and 207 cm^{-1} in the 80 K study by Buckley and Clark [12]. These workers follow the assignment of these bands, as due to excitations of t_{2g}, t_{2g} and e_g modes (vibrations ν_{23}, ν_{24} and ν_9) respectively, by Rocchiccioli-Deltcheff et al. [18] based on their normal coordinate analysis and isotopic shifts. However, each of the computational methods predicts that ν_9 is actually the

Table 4
Calculated and experimental vibrational frequencies (in cm^{-1}) and assignments for $[Mo_6O_{19}]^{2-}$ at the BLYP level

Mode		Experimental			Basis set		
		[12]	[16]	[18]	**A**	**B**	**C**
a_{1g}	ν_1	987	980	986	940	937	938
e_g	ν_6	954	951	958	909	910	910
t_{1u}	ν_{14}		957	956	908	909	910
e_g	ν_7	810	809	817	737	742	746
t_{1u}	ν_{15}		798	796	730	741	742
t_{2g}	ν_{21}				541	529	528
t_{1u}	ν_{16}		602	598	541	538	538
a_{1g}	ν_2	597	580	598	515	498	498
t_{2u}	ν_{25}				487	485	483
t_{2u}	ν_{26}				439	442	449
t_{1g}	ν_{11}				449	460	468
a_{2g}	ν_4				410	410	423
e_g	ν_8	440			448	439	439
t_{1u}	ν_{17}		438	432	421	424	425
a_{2u}	ν_5				439	453	459
t_{2g}	ν_{22}	329			412	424	429
t_{1u}	ν_{18}		356	352	342	363	360
a_{1g}	ν_3	286	278	285	276	277	276
e_u	ν_{10}				266	273	276
t_{1g}	ν_{12}				220	216	217
t_{2g}	ν_{23}	200	163	205	216	212	216
t_{1u}	ν_{19}		220	217	204	202	201
t_{1u}	ν_{20}		192		185	187	189
t_{2u}	ν_{27}				188	179	186
t_{2g}	ν_{24}	166	125	166	192	184	186
e_g	ν_9	207	197		145	148	149
t_{2u}	ν_{28}				124	126	131
t_{1g}	ν_{13}				81	53	55
RMS error assignment 1					47	48	47
RMS error assignment 2					47	48	47

The RMS error is calculated with respect to the data from [18].

lowest Raman active vibration. Assignment 2 thus associates the band at 166 cm^{-1} to an e_g vibration. The calculated Raman intensity of these low frequency e_g and t_{2g} modes are all quite low and similar and do not allow an unambiguous assignment. These modes involve Mo–O_b stretching and are all likely to be sensitive to isotopic substitution. The second major source of error is in the frequency of the Raman active a_{1g} mode at ca. 598 cm^{-1}. This band is, experimentally, relatively broad and there is a little discrepancy in the position in the experimental reports. However, the intensity and reported polarization of the Raman peak suggest that it is correctly assigned by Rocchiccioli-Deltcheff et al. [18].

The results of the HF calculations are considerably poorer than those of the DF methods. Whilst the overbinding that results from the absence of correlation in the HF calculations acts to compensate for the lack of a crystal field in the treatment of the geometry, it is apparent in the inaccuracy of the vibrational frequencies. The errors are most notable in the high frequency region for the modes that are predominately Mo–O_t stretching in character with ca. 10% overestimation of values. The DF methods all perform extremely well in this region. The relative performance of the DF methods mirrors the treatment of the geometry. The most accurate modelling of the experimental frequencies is ob-

Table 5
Calculated and experimental vibrational frequencies (in cm^{-1}) and assignments for $[Mo_6O_{19}]^{2-}$ at the B3LYP level

Mode		Experimental			Basis set	
		[12]	[16]	[18]	**B**	**C**
a_{1g}	ν_1	987	980	986	999	999
e_g	ν_6	954	951	958	968	968
t_{1u}	ν_{14}		957	956	969	970
e_g	ν_7	810	809	817	803	804
t_{1u}	ν_{15}		798	796	802	800
t_{2g}	ν_{21}				566	563
t_{1u}	ν_{16}		602	598	571	570
a_{1g}	ν_2	597	580	598	527	526
t_{2u}	ν_{25}				514	510
t_{2u}	ν_{26}				450	460
t_{1g}	ν_{11}				481	489
a_{2g}	ν_4				408	426
e_g	ν_8	440			465	462
t_{1u}	ν_{17}		438	432	454	454
a_{2u}	ν_5				484	490
t_{2g}	ν_{22}	329			451	456
t_{1u}	ν_{18}		356	352	379	376
a_{1g}	ν_3	286	278	285	295	294
e_u	ν_{10}				288	291
t_{1g}	ν_{12}				227	229
t_{2g}	ν_{23}	200	163	205	228	231
t_{1u}	ν_{19}		220	217	213	212
t_{1u}	ν_{20}		192		199	201
t_{2u}	ν_{27}				187	194
t_{2g}	ν_{24}	166	125	166	195	197
e_g	ν_9	207	197		156	157
t_{2u}	ν_{28}				124	131
t_{1g}	ν_{13}				109	68
RMS error assignment 1					27	27
RMS error assignment 2					25	25

The RMS error is calculated with respect to the data from [18].

tained at the LDA level with the STO/ZORA approach. The LDA and B3LYP results for the GTO basis sets are somewhat less accurate. The BP86 and BLYP results are significantly poorer. It is noticeable that, whilst above it was suggested that the overbinding associated with the LDA and HF methods probably acts to compensate for the absence of a crystal field in these calculations, the local density approach is able to accurately model *both* the geometry and vibrational frequencies. The calculations on the remainder of the Lindqvist anions were thus performed at the LDA level with the STO/ZORA approach. It has been noted previously that gradient corrections do not necessarily lead to an increase, and often lead to a decrease, in the accuracy of DF calculated vibrational frequencies [52]. Stückl et al. have reported geometries for transition metal MO_4 ions and molecules at the LDA and gradient corrected levels. The LDA geometries of both the neutral and highly anionic systems were found to be consistently closer to experiment than those obtained using gradient corrected functionals. As a result, these authors reported vibrational frequencies at the LDA level only.

3.3. Vibrational spectrum of the $[W_6O_{19}]^{2-}$ anion

The calculated structure of $[W_6O_{19}]^{2-}$ at the LDA level with the STO/ZORA approach has

Table 6
Calculated and experimental vibrational frequencies (in cm^{-1}) and assignments for $[Mo_6O_{19}]^{2-}$ at the HF level

Mode		Experimental			Basis set	
		[12]	[16]	[18]	**B**	**C**
a_{1g}	ν_1	987	980	986	1143	1142
e_g	ν_6	954	951	958	1093	1094
t_{1u}	ν_{14}		957	956	1099	1100
e_g	ν_7	810	809	817	926	919
t_{1u}	ν_{15}		798	796	636	634
t_{2g}	ν_{21}				633	626
t_{1u}	ν_{16}		602	598	521	519
a_{1g}	ν_2	597	580	598	585	584
t_{2u}	ν_{25}				514	564
t_{2u}	ν_{26}				440	466
t_{1g}	ν_{11}				509	522
a_{2g}	ν_4				385	437
e_g	ν_8	440			504	501
t_{1u}	ν_{17}		438	432	404	414
a_{2u}	ν_5				569	570
t_{2g}	ν_{22}	329			451	456
t_{1u}	ν_{18}		356	352	379	401
a_{1g}	ν_3	286	278	285	342	339
e_u	ν_{10}				326	326
t_{1g}	ν_{12}				265	268
t_{2g}	ν_{23}	200	163	205	259	259
t_{1u}	ν_{19}		220	217	239	238
t_{1u}	ν_{20}		192		222	223
t_{2u}	ν_{27}				208	216
t_{2g}	ν_{24}	166	125	166	225	225
e_g	ν_9	207	197		169	172
t_{2u}	ν_{28}				111	142
t_{1g}	ν_{13}				99	89
RMS error assignment 1					95	96
RMS error assignment 2					94	94

The RMS error is calculated with respect to the data from [18].

previously been reported and compared to the available experimental results [35]. The assumed octahedral symmetry of this anion is confirmed by the vibrational analyses reported here. The accuracy of the calculated structure of $[W_6O_{19}]^{2-}$ is similar to that described above for the molybdenum analogue with the ZORA approach able to reproduce the observed *decrease* in metal–oxygen bond lengths between molybdenum and tungsten.

Table 7 lists the calculated vibrational frequencies for $[W_6O_{19}]^{2-}$ at the same level of theory, together with a comparison with the available experimental results. The RMS error is higher than that obtained for $[Mo_6O_{19}]^{2-}$ at the same level of theory. The assignment of the lowest frequency Raman active modes is again uncertain. Assignment 1 follows that of von Mattes et al. [16] with the bands at 122 and 178 cm^{-1} assigned to t_{2g} (ν_{28}) and e_g (ν_9), respectively. The calculated frequencies strongly suggest a reversal of this assignment. The RMS error for this assignment (2) is reduced considerably.

3.4. Vibrational spectrum of the reduced $[Mo_6O_{19}]^{3-}$ anion

The lowest unoccupied orbitals for the $[Mo_6O_{19}]^{2-}$ anion is an e_u function. As described in detail elsewhere [35], this orbital is weakly Mo–O_b antibonding in character and becomes occupied

Table 7
Calculated and experimental vibrational frequencies (in cm^{-1}) and assignments for $[W_6O_{19}]^{2-}$ at the VWN level

Mode		Experimental [16]	Calculated
a_{1g}	ν_1	992	1051
e_g	ν_6	968	1029
t_{1u}	ν_{14}	972	1029
e_g	ν_7	836	870
t_{1u}	ν_{15}	812	848
t_{1u}	ν_{16}	586	596
t_{2g}	ν_{21}	658	584
a_{2g}	ν_4		611
t_{2u}	ν_{25}		605
a_{1g}	ν_2	557	576
t_{1g}	ν_{11}		570
t_{2u}	ν_{26}		540
e_g	ν_8	501	512
a_{2u}	ν_5		455
t_{1u}	ν_{17}	444	448
t_{2g}	ν_{22}		417
t_{1u}	ν_{18}	369	356
e_u	ν_{10}		269
a_{1g}	ν_3	230	233
t_{1g}	ν_{12}		204
t_{1u}	ν_{19}	226	185
t_{2g}	ν_{23}	215	176
t_{2u}	ν_{27}		179
t_{2g}	ν_{24}	122	173
t_{1u}	ν_{20}	174	169
t_{1g}	ν_{13}		148
e_g	ν_9	178	126
t_{2u}	ν_{28}		114
RMS error assignment 1			40
RMS error assignment 2			36

The RMS error is calculated with respect to the data from [18].

when the anion is reduced. Single occupation of this orbital in an octahedral $[Mo_6O_{19}]^{3-}$ system leads to a ^2E_u ground term which is Jahn–Teller active along e_g modes. Previous workers [12,19] have assumed that the electron is localized on one metal atom to give a mixed valence $[Mo^{V}Mo^{VI}_5O_{19}]^{3-}$ anion with C_{4v} symmetry. Our previous treatment of the reduced anion have been performed starting from geometries of C_{2v} and C_{4v} symmetry to allow for the possibility of charge localization and delocalization along the Jahn–Teller active modes. Small distortions are predicted to give C_{4v} structures in $^2A_2$ or $^2B_2$ states corresponding to a slight tetragonally elongation or compression, respectively, of the parent octahedral cluster. In fact, the structures of the reduced anions are close to D_{4h}. The structural and energetic differences between these two states, however, were predicted to be small with effective delocalization of the electron. The numbering system of the atoms is shown in Fig. 2(a).

The effect of descending in symmetry from O_h to C_{4v} on the symmetry and IR/Raman activity of

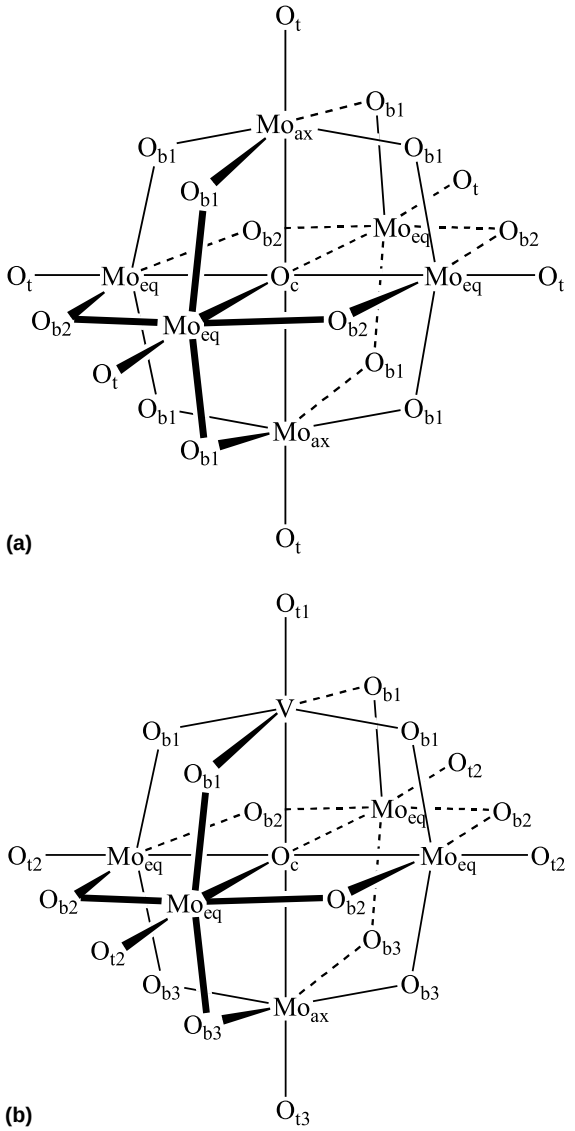

Fig. 2. Structure and labelling of C_{4v} (a) reduced $[Mo_6O_{19}]^{3-}$ and (b) metal substituted $[VMo_5O_{19}]^{n-}$ ($n = 3, 4$) polyanions.

the 69 normal modes of vibration is shown in Table 8. In O_h symmetry, there are seven IR active modes and 11 Raman active modes. Lowering of the symmetry to C_{4v} leads, in principle, to 32 IR active modes and 42 Raman active modes. If only the modes which are active in O_h are observed, seven IR and 16 Raman modes might be expected. Tables 9 and 10 list the calculated frequencies for the $^2A_2$ or $^2B_2$ states of $[Mo_6O_{19}]^{3-}$ together with a comparison with the experimental results of Rocchiccioli-Deltcheff et al. [19]. The bands have been assigned by reference to the calculated IR intensity and the observed activity. The previous assignment by Rocchiccioli-Deltcheff et al. utilized the forcefield of the oxidized O_h $[Mo_6O_{19}]^{2-}$ anion.

Table 8
Effect of descent in symmetry from O_h to C_{4v} on the symmetry and IR/Raman activity of the normal modes of a Lindqvist polyanion

Octahedral		C_{4v}
$3a_{1g}(R)$	→	$3a_1(IR, R)$
$a_{2g}(R)$	→	$b_1(R)$
$4e_g(R)$	→	$4a_1(IR, R) + 4b_1(R)$
$3t_{1g}$	→	$3a_2 + 3e(IR, R)$
$4t_{2g}(R)$	→	$4b_2(R) + 4e(IR, R)$
a_{2u}	→	$b_2(R)$
e_u	→	$a_2 + b_2(R)$
$7t_{1u}(IR)$	→	$7a_1(IR, R) + 7e(IR, R)$
$4t_{2u}$	→	$4b_1(R) + 4e(IR, R)$
Total		$14a_1$ (IR, R) + $4a_2 + 9b_1(R) + 6b_2(R)$ + 18e(IR, R)

The vibrational spectra of the two states are quite similar in many regions. The high frequency region of the spectra corresponds to Mo–O_t and Mo–O_b stretching motions. Table 11 shows the effect of reduction on this region. Studies of $[MoOCl_5]^{n-}$ ($n = 1$ for Mo(VI) and $n = 2$ for Mo(V)) complexes which are simple models of

Table 9
Calculated and experimental vibrational frequencies (in cm^{-1}) and assignments for the $^2A_2$ state of the $[Mo_6O_{19}]^{3-}$ ion at the VWN level

Mode		Experimental [19]	Calculated	Mode		Experimental [19]	Calculated
a_1	ν_1	970 (R, m)	963	b_2	ν_{30}		406
b_1	ν_{19}	937 (R, w)	929	a_1	ν_{10}	358 (IR, w)	376 (10)
a_1	ν_2	938 (IR, vs)	929 (256)	a_1	ν_{11}	283 (IR, vw)	285 (1)
e	ν_{34}		929 (662)	b_2	ν_{31}		278
a_1	ν_3		927 (432)	a_2	ν_{16}		238
a_1	ν_4		797	e	ν_{43}	220 (IR, w)	227 (2)
a_1	ν_5	780 (IR, vs)	789 (649)	b_2	ν_{32}		224
e	ν_{35}		583	e	ν_{44}		223
b_2	ν_{28}		575	a_2	ν_{17}		221
e	ν_{36}		570	e	ν_{45}	205 (R, vw)	215
a_1	ν_6	616 (IR, m)	557 (69)	a_1	ν_{12}		203 (1)
e	ν_{37}		557 (118)	e	ν_{46}	189 (IR, w)	199 (10)
e	ν_{38}	565 (IR, m)	541 (13)	b_1	ν_{24}		196
b_1	ν_{20}	548 (R, w)	536	b_2	ν_{33}		193
a_1	ν_7		534	e	ν_{47}		192
a_2	ν_{15}		514	e	ν_{48}		190 (3)
b_1	ν_{21}		511	a_1	ν_{13}	150 (IR, w)	188 (12)
b_1	ν_{22}		500	a_2	ν_{18}		167
e	ν_{39}		494	b_1	ν_{25}		163
e	ν_{40}		481 (12)	a_1	ν_{14}		153
a_1	ν_8		468	e	ν_{49}		143
a_1	ν_9	450 (IR, s)	455 (155)	b_1	26		141
b_1	ν_{23}		437	e	ν_{50}		124
b_2	ν_{29}		437	b_1	ν_{27}		123
e	ν_{41}		416	e	ν_{51}		103 (5)
e	ν_{42}	418 (IR, s)	411 (115)				

Calculated IR intensities (km mol^{-1}) and experimental activity (vs = very strong, s = strong, m = medium, w = weak and vw = very weak) are also indicated.

Table 10
Calculated and experimental vibrational frequencies (in cm^{-1}) and assignments for the $^2B_2$ state of the $[Mo_6O_{19}]^{3-}$ ion at the VWN level

Mode		Experimental [19]	Calculated	Mode		Experimental [19]	Calculated
a_1	ν_1	970 (R, m)	963	e	ν_{42}		409
a_1	ν_2	938 (IR, vs)	930 (500)	e	ν_{43}	358 (IR, w)	325 (12)
a_1	ν_3		929 (164)	a_1	ν_{10}	283 (IR, vw)	285 (1)
e	ν_{34}		928 (667)	a_2	ν_{16}		278
b_1	ν_{19}	937 (R, w)	928	b_2	ν_{31}		238
a_1	ν_4		766	a_2	ν_{17}		224
e	ν_{35}	780 (IR, vs)	691 (220)	e	ν_{44}		222
b_1	ν_{20}		580	e	ν_{45}		219
e	ν_{36}		575	a_1	ν_{11}	220 (IR, w)	214 (2)
b_2	ν_{28}		566	b_2	ν_{32}	205 (R, w)	214
a_1	ν_5	615 (IR, m)	563 (58)	e	ν_{46}	189 (IR, w)	205 (4)
b_1	ν_{21}	548 (R, w)	561	b_1	ν_{24}		197
e	ν_{37}	565 (IR, m)	557 (100)	e	ν_{47}		193
a_1	ν_6		534	b_2	ν_{33}		191
a_1	ν_7		519 (1)	a_1	ν_{12}		189
b_1	ν_{22}		517	e	ν_{48}	150 (IR, vw)	188 (11)
e	ν_{38}		516 (5)	e	ν_{49}		186
e	ν_{39}		506	b_1	ν_{25}		177
b_1	ν_{23}		504	e	ν_{50}		162
a_2	ν_{15}		492	b_1	ν_{26}		155
e	ν_{40}	450 (IR, s)	469 (43)	b_1	ν_{27}		148
a_1	ν_8		453	a_1	ν_{13}		145
b_2	ν_{29}		437	e	ν_{51}		130
b_2	ν_{30}		420	a_1	ν_{14}		90 (2)
a_1	ν_9	418 (IR, s)	414 (115)	a_2	ν_{18}		77
e	ν_{41}		413 (123)				

Calculated IR intensities (km mol^{-1}) and experimental activity (vs = very strong, s = strong, m = medium, w = weak and vw = very weak) are also indicated.

Table 11
Effect of reduction and substitution on the high frequency vibrational modes (cm^{-1}) of $[Mo_6O_{19}]^{2-}$, $[Mo_6O_{19}]^{3-}$, $[VMo_5O_{19}]^{3-}$ and $[VMo_5O_{19}]^{4-}$

$[Mo_6O_{19}]^{2-}$ $^1A_1$	$[Mo_6O_{19}]^{3-}$ $^2A_2$	$[Mo_6O_{19}]^{3-}$ $^2B_2$	$[VMo_5O_{19}]^{3-}$ $^1A_1$	$[VMo_5O_{19}]^{4-}$ $^2B_2$	Approximate description[a]
$993(a_{1g})$	$963(a_1)$	$963(a_1)$	$1008(a_1)$	$971(a_1)$	$\nu(M–O_t)$
$963(e_g)$	$929(a_1) + 929(b_1)$	$929(a_1) + 927(b_1)$	$948(a_1) + 923(b_1)$	$913(a_1) + 886(b_1)$	$\nu(M_{ax}–O_t)$ $\nu(M_{eq}–O_t)$
$962(t_{1u})$	$929(e) + 927(a_1)$	$929(e) + 927(a_1)$	$923(e) + 920(a_1)$	$885(e) + 881(a_1)$	$\nu(M_{eq}–O_t)$ $\nu(M_{ax}–O_t)$
$806(e_g)$	$797(a_1) + 536(b_1)$	$766(a_1) + 580(b_1)$	$807(a_1) + 798(b_1)$	$756(a_1) + 645(b_1)$	$\nu(M_{ax}–O_b)$ $\nu(M_{eq}–O_b)$
$799(t_{1u})$	$583(e) + 789(a_1)$	$691(e) + 563(a_1)$	$791(e) + 783(a_1)$	$697(e) + 559(a_1)$	$\nu(M_{eq}–O_b)$ $\nu(M_{ax}–O_b)$

[a] ax refers to metal atoms along the C_4 axis of the C_{4v} ions and eq refers to the metal atoms not on the C_4 axis. For the $[VMo_5O_{19}]$ ions, $M_{ax} = V$ and Mo_{ax}.

Type I polyanions give values of 953 cm^{-1} for $\nu(Mo^{VI}–O_t)$ and 949 cm^{-1} for $\nu(Mo^{V}–O_t)$ [34]. In the polyanion, the effect of reduction on the magnitude of $\nu(Mo–O_t)$ is ca. 30 cm^{-1} but the splitting of the O_h bands due to the lowering of symmetry is ca. 2 cm^{-1} or less.

There are larger effects on the $Mo–O_b$ stretching modes on reduction. It is in this region that the largest differences between the spectra of the $^2A_2$ and $^2B_2$ states occur leading to different assignments of the bands derived from the very strong IR $\nu_{15}(t_{1u})$ band at ca. 798 cm^{-1} in the oxidized

anion. In the IR spectrum of the reduced polyanion, a strong absorption is observed at ca. 780 cm^{-1}. In the calculated spectrum of the $^2A_2$ state, the nearest strong absorption is the $\nu_5(a_1)$ mode at 789 cm^{-1}. The nearest strong absorption in the calculated spectrum of the $^2B_2$ state, however, is the $\nu_{35}(e)$ mode at 691 cm^{-1}. In the spectra of the $^2A_2$ and $^2B_2$ states, there are shifts to lower frequencies and splittings of the $\nu_{15}(t_{1u})$ and nearby $\nu_7(e_g)$ modes. As discussed in detail previously [34,35], the singly occupied orbital in the reduced systems is Mo–O_b anti-bonding but Mo–O_t non-bonding in character so that the effect of reduction is most noticeable on modes involving the former. The $\nu_{15}(t_{1u})$ band in the parent octahedral system splits into the $\nu_5(a_1)$ and $\nu_{35}(e)$ bands in the reduced systems. ν_5 lies well above ν_{35} in the $^2A_2$ state and the splitting is reversed in the $^2B_2$ state. The $\nu_5(a_1)$ mode is dominated by stretching of the Mo_{ax}–O_{b1} bonds. The $\nu_{35}(e)$ mode is dominated by stretching of the Mo_{eq}–O_{b1} and Mo_{eq}–O_{b2} bonds.

In the $^2A_2$ state, the unpaired electron lies in an a_2 orbital which is antibonding with respect to the Mo_{eq}–O_{b1} bonds. As a result, there is an elongation along the C_4 axis: the Mo_{eq}–O_{b1} bond length increases from 1.93 Å in $[Mo_6O_{19}]^{2-}$ to 1.95 Å in the $^2A_2$ state of $[Mo_6O_{19}]^{3-}$ whilst the Mo_{ax}–O_{b1} bond length actually decreases slightly from 1.93 to 1.92 Å. The frequency of the $\nu_{35}(e)$ mode is thus decreased much more than that of the $\nu_5(a_1)$ mode. As the Mo_{ax}–O_{b1} bonding appears to be little affected by reduction, the frequency of the $\nu_5(a_1)$ mode is decreased only slightly.

In the $^2B_2$ state, the unpaired electron lies in a b_2 orbital which is antibonding with respect to the Mo_{ax}–O_{b1} and Mo_{eq}–O_{b2} bonds. Elongation therefore occurs perpendicular to the C_4 axis and leads to a slight compression along the C_4 axis: the Mo_{ax}–O_{b1} and Mo_{eq}–O_{b2} bond lengths increase from 1.93 Å in $[Mo_6O_{19}]^{2-}$ to 1.94 Å in the $^2B_2$ state of $[Mo_6O_{19}]^{3-}$ whilst the Mo_{eq}–O_{b1} bond length is essentially unchanged. The frequency of the $\nu_5(a_1)$ mode is thus decreased much more than that of the $\nu_{35}(e)$ mode. As population of the b_2 orbital weakens the bonding of Mo_{ax}–O_{b1} and Mo_{eq}–O_{b2} connections, the frequency of the $\nu_{35}(e)$ mode is decreased by reduction. The subsequent absence of a calculated band for the $^2B_2$ state of $[Mo_6O_{19}]^{3-}$ to match the strong IR absorption at ca. 780 cm^{-1} suggests that it is $^2A_2$ state which is observed experimentally. In the gas-phase, the energy difference between the $^2A_2$ and $^2B_2$ states at the LDA and at the BP86 level (both calculated using the LDA geometry) is negligible. Any preference for the $^2A_2$ state must arise from the environment in the experimental system.

3.5. Structure and vibrational spectra of $[VMo_5O_{19}]^{3-}$ and $[VMo_5O_{19}]^{4-}$ anions

The Raman spectra of $[VMo_5O_{19}]^{3-}$ and $[VMo_5O_{19}]^{4-}$ have been reported by Buckley and Clark [12]. No crystallographic study of these anions appears to have been reported. Table 12 lists the calculated bond lengths and Mulliken charges for these anions using the atom numbering scheme from Fig. 2(b). The geometry optimizations were performed starting from C_{2v} and C_{4v} configurations. The lowest state of the reduced anion is $^2B_2$ with the $^2A_2$ state lying ca. 50 kJ mol^{-1} higher in

Table 12
M–O bond lengths (Å) and Mulliken charges (spin densities) for $[VMo_5O_{19}]^{3-}$ and for the $^2B_2$ state of $[VMo_5O_{19}]^{4-}$

	$[VMo_5O_{19}]^{3-}$	$[VMo_5O_{19}]^{4-}$
Bond lengths		
V–O_c	2.324	2.341
V–O_{b1}	1.878	1.909
V–O_{t1}	1.611	1.628
Mo_{eq}–O_c	2.313	2.329
Mo_{eq}–O_{b1}	1.876	1.868
Mo_{eq}–O_{b2}	1.931	1.948
Mo_{eq}–O_{b3}	1.951	1.948
Mo_{eq}–O_{t2}	1.730	1.747
Mo_{ax}–O_c	2.259	2.266
Mo_{ax}–O_{b3}	1.926	1.944
Mo_{ax}–O_{t3}	1.733	1.749
Charges (*spin densities*)		
V	1.51	1.42 (0.43)
Mo_{eq}	2.17	2.08 (0.04)
Mo_{ax}	2.13	2.03 (0.18)
O_c	−1.17	−1.16
O_{b1}	−0.79	−0.80
O_{b2}	−0.84	−0.86 (0.08)
O_{b3}	−0.84	−0.85
O_{t1}	−0.64	−0.73 (0.04)
O_{t2}	−0.72	−0.77
O_{t3}	−0.72	−0.77

energy at the BP86 level (calculated with the LDA geometry). The geometry optimizations and subsequent vibrational analyses confirm that both ions have C_{4v} symmetry. A detailed study of the bonding and the effects of reduction on the electronic structure will be reported elsewhere. The Mulliken charges, which have been shown previously to give qualitatively similar results to those from other population analyses for polyanions [32], suggest that the additional electron is delocalized over all the metal atoms in $[VMo_5O_{19}]^{4-}$. The reduced species does not contain V^{IV} and Mo^{VI} as previously suggested [12].

Tables 13 and 14 list the vibrational frequencies and assignments for $[VMo_5O_{19}]^{3-}$ and $[VMo_5O_{19}]^{4-}$. The symmetry and IR/Raman activity of the vibrations are shown in Table 8. Only the Raman spectra have been published [12] and these are included in Tables 13 and 14 for comparison. The agreement between the calculated and observed frequencies is very good for $[VMo_5O_{19}]^{3-}$. Experimentally, the bands in the high frequency region appear to shift to higher frequency upon reduction despite the reduction in the oxidation states of the metal ions. The calculated frequencies, however, *decrease* in energy upon reduction. This is probably associated with the high negative charge (−4) associated with this reduced polyanion and the inadequacy of the gas-phase treatment.

As well as detailing the effect of reducing $[Mo_6O_{19}]^{2-}$, Table 11 shows the consequences of replacing an Mo^{VI} atom with a V^{V} atom and of reducing $[VMo_5O_{19}]^{3-}$ to $[VMo_5O_{19}]^{4-}$ on the high frequency vibrational modes. As noted above, the Mo–O_t stretching modes are reduced in frequency by reduction but there is minimal splitting of the degenerate modes. Replacement of Mo^{VI} by V^{V}, however, causes much larger splitting of these modes as might be expected from the greater

Table 13
Calculated and experimental vibrational frequencies (in cm^{-1}) and assignments for the $[VMo_5O_{19}]^{3-}$ ion at the VWN level

Mode		Experimental [12]	Calculated	Mode		Experimental [12]	Calculated
a_1	ν_1	976	1008 (290)	e	ν_{43}		420
a_1	ν_2	949	948 (141)	b_2	ν_{30}		417
b_1	ν_{19}	930	923	a_1	ν_{10}		364 (4)
e	ν_{34}		923 (623)	e	ν_{43}		358 (2)
a_1	ν_3		920 (306)	a_1	ν_{11}	292	296
a_1	ν_4	799	807 (252)	a_2	ν_{16}		279
b_1	ν_{20}		798	b_2	ν_{31}		269
e	ν_{35}	775	791 (605)	e	ν_{44}		242
a_1	ν_5	740	783 (333)	e	ν_{45}		229
e	ν_{36}		612 (51)	a_1	ν_{12}	207	224
b_2	ν_{28}		579	a_2	ν_{17}		221
e	ν_{37}		573 (56)	b_2	ν_{32}		221
a_1	ν_6	586	566 (52)	e	ν_{46}		215 (2)
b_1	ν_{21}		558	b_1	ν_{25}		205
a_1	ν_7		534 (4)	a_1	ν_{13}		205 (7)
e	ν_{38}		527 (1)	e	ν_{47}		201 (4)
a_2	ν_{15}		507	e	ν_{48}		197 (2)
e	ν_{39}		503 (1)	b_2	ν_{33}		196
b_1	ν_{22}		497	e	ν_{49}		192
e	ν_{40}		480 (1)	a_1	ν_{14}	163	163
b_1	ν_{23}		477	b_1	ν_{26}		152
a_1	ν_8		470	e	ν_{50}		138
e	ν_{41}		450 (180)	b_1	ν_{27}		137
a_1	ν_9	450	448 (169)	a_2	ν_{18}		75
b_2	ν_{29}		445	e	ν_{51}		69
b_1	ν_{24}		434				

Calculated IR intensities (km mol^{-1}) are shown in parentheses.

Table 14
Calculated and experimental vibrational frequencies (in cm^{-1}) and assignments for the $^2B_2$ state of the $[VMo_5O_{19}]^{4-}$ ion at the VWN level

Mode		Experimental [12]	Calculated	Mode		Experimental [12]	Calculated
a_1	ν_1	1006	971 (312)	e	ν_{42}	363	405 (98)
a_1	ν_2	957	913 (171)	e	ν_{43}	353	336 (4)
b_1	ν_{19}		886	b_1	ν_{24}		334
e	ν_{34}		885 (778)	a_1	ν_{10}	313	289
a_1	ν_3	946	881 (333)	a_2	ν_{16}		284
a_1	ν_4	795	756	e	ν_{44}		245
e	ν_{35}	742	697 (179)	b_2	ν_{31}		240
b_1	ν_{20}		645	a_1	ν_{11}	213	231
b_1	ν_{21}		589	e	ν_{45}		228
e	ν_{36}		586 (72)	a_2	ν_{17}		223
a_1	ν_5		559 (56)	b_2	ν_{32}		214
b_2	ν_{28}		557	e	ν_{46}		208 (7)
e	ν_{37}		552 (97)	a_1	ν_{12}		206
a_1	ν_6	589	543 (19)	e	ν_{47}		202 (2)
b_1	ν_{22}		506	b_1	ν_{25}		196
e	ν_{38}		502 (1)	b_2	ν_{33}		190
a_1	ν_7		502	e	ν_{48}		189 (3)
e	ν_{39}		497 (2)	e	ν_{49}		185 (5)
a_2	ν_{15}		486	a_1	ν_{13}		173 (9)
b_1	ν_{23}		474	e	ν_{50}		154
e	ν_{40}		458 (85)	a_1	ν_{14}	163	151 (1)
b_2	ν_{29}		440	b_1	ν_{26}		149
a_1	ν_8	457	438 (12)	b_1	ν_{27}		133
b_2	ν_{30}		421	e	ν_{51}		133
a_1	ν_9		420 (139)	a_2	ν_{18}		61
e	ν_{41}		415 (29)				

Calculated IR intensities (km mol^{-1}) are shown in parentheses.

structural perturbation. The V^V–O_t stretching frequency in the model system $[VOCl_5]^{2-}$ is 1023 cm^{-1} and is ca. 70 cm^{-1} higher than the Mo^{VI}–O_t frequency in the molybdenum analogue [34]. The effect on the frequency of the $\nu_1(a_1)$ metal-oxo "breathing mode" in the polyanion is somewhat smaller, increasing from 993 cm^{-1} in $[Mo_6O_{19}]^{2-}$ to 1008 cm^{-1} in $[VMo_5O_{19}]^{3-}$. Reduction of $[VMo_5O_{19}]^{3-}$ causes a decrease in metal-oxo stretching frequencies but no significant increase in the splittings, reflecting the metal-oxo non-bonding character of the singly occupied orbital in $[VMo_5O_{19}]^{4-}$.

As noted above, the effect of reducing $[Mo_6O_{19}]^{2-}$ is most profound on the frequencies of the Mo–O_b stretching modes with large splitting of the $\nu_{15}(t_{1u})$ band. Replacement of Mo^{VI} by V^V, however, causes only a small splitting of these modes reflecting the insignificant changes to the Mo_{eq}–O_{b2}, Mo_{eq}–O_{b3} and Mo_{ax}–O_{b3} bond lengths. Reduction of $[VMo_5O_{19}]^{3-}$, however, has a very similar effect to that described above for $[Mo_6O_{19}]^{2-}$. The singly occupied orbital in the $^2B_2$ state occupies a b_2 orbital which is antibonding with respect to the V-O_{b1}, Mo_{ax}–O_{b3} and Mo_{eq}–O_{b2} bonds causing these bonds to lengthen whilst the other bridging bonds actually shorten slightly. The effect on the structure and on the frequencies is thus entirely analogous to that described above for the $^2B_2$ state of $[Mo_6O_{19}]^{3-}$ with the frequency of the $\nu_5(a_1)$ mode decreased much more than that of the ν_{35}(e) mode.

4. Conclusions

The structures and vibrational spectra of the Lindqvist polyanions $[Mo_6O_{19}]^{2-}$, $[W_6O_{19}]^{2-}$,

$[Mo_6O_{19}]^{3-}$, $[VMo_5O_{19}]^{3-}$ and $[VMo_5O_{19}]^{4-}$ have been calculated using density functional theory. For $[Mo_6O_{19}]^{2-}$, a detailed comparison between the performance of commonly used functionals and basis sets and between Hartree–Fock and density functional methods has been performed. The Hartree–Fock method appears to reproduce structural parameters but performs very poorly when applied to the vibrational frequencies. The results suggest that the local density approximation with Slater type orbitals and the ZORA approach is best able to model both the structure and vibrational spectra of these polyanions when treated as pseudo-gas phase species. These calculations are extremely computationally demanding requiring precise energies and geometries and cannot yet be considered a standard task for the study of these large, heavy element cluster anions.

The vibrational analyses confirm the high symmetry for these anions suggested by previous geometry optimizations with O_h symmetry for $[Mo_6O_{19}]^{2-}$ and $[W_6O_{19}]^{2-}$ and C_{4v} symmetry for the reduced and metal substituted systems. Reduction of $[Mo_6O_{19}]^{2}$ gives rise to $^2A_2$ and $^2B_2$ states of $[Mo_6O_{19}]^{3-}$ with the computational results for the former most closely matching the previously reported vibrational spectra. Reduction causes only small effects on the stretching frequencies of the terminal Mo–O bonds confirming the non-bonding character of the singly occupied orbital with respect to these bonds. There is no evidence for the formation of a localized Mo(V) atom and a mixed-valency in either state of $[Mo_6O_{19}]^{3-}$. The antibonding character of the singly occupied orbital with respect to the bridging Mo–O bonds, however, is confirmed by the large splitting of the respective stretching modes. Replacement of an Mo(VI) for a V(V) atom causes a more significant splitting of the stretching frequencies of the terminal metal-oxo bonds with a much smaller effect on the bridging bonds. However, the effect of reduction on the vibrational spectrum of $[VMo_5O_{19}]^{3-}$ is entirely analogous to that of reducing $[Mo_6O_{19}]^{2-}$ with minimal changes to the terminal metal-oxo bonds and large splitting of the stretching frequencies of the bridging bonds.

Acknowledgements

The authors would like to thank EPSRC, the Cambridge Overseas Trust, Selwyn College (Cambridge) and the University of Hull for financial support, the UK Computational Chemistry Working Party for access to computational facilities in the Rutherford Appleton Laboratory and Dr. Nigel Young of the University of Hull for useful discussions.

References

[1] M.T. Pope, Heteropoly and Isopoly Oxometalates, Springer, Heidelberg, 1983.
[2] M.T. Pope, A. Müller, Angew. Chem. Int. Ed. Engl. 30 (1991) 34.
[3] L.C.W. Baker, D.C. Glick, Chem. Rev. 98 (1998) 3.
[4] M.T. Pope, A. Müller, Polyoxometalates: From Platonic Solids to Anti-Retroviral Activity, Kluwer Academic Press, Dordrecht, 1994.
[5] I. Lindqvist, Ark. Kemi. 5 (1952) 247.
[6] I. Lindqvist, B. Aronsson, Ark. Kemi. 7 (1954) 49.
[7] W. Clegg, G.M. Sheldrick, C.D. Garner, I.B. Walton, Acta Crystallogr. B 38 (1982) 2906.
[8] J. Fuchs, W. Freiwald, H. Hartl, Acta Crystallogr. B 34 (1978) 1764;
C. Ming-Quin, Z. Si-San, G. Yi-Dong, J. Struct. Chem. 9 (1990) 26.
[9] K.H. Tytko, J. Mehmke, S. Fischer, Struct. Bond. 93 (1990) 129.
[10] M. Dabbabi, M. Boyer, Inorg. Nucl. Chem. 38 (1976) 1011.
[11] W.G. Klemperer, W. Shun, J. Am. Chem. Soc. 100 (1978) 4891.
[12] R.I. Buckley, R.J.H. Clark, Coord. Chem. Rev. 65 (1985) 167.
[13] C. Sanchez, J. Livage, J.P. Launay, M. Fournier, Y. Jeannin, J. Am. Chem. Soc. 104 (1982) 3194.
[14] K. Piepgrass, J.N. Barrows, M.T. Pope, J. Chem. Soc., Chem. Commun. (1989) 10.
[15] E.B. Wilson, J.C. Decius, P.C. Cross, Molecular Vibrations, McGraw-Hill, New York, 1955.
[16] R. von Mattes, H. Bierbüsse, J. Fuchs, Z. Anorg. Allgem. Chem. 385 (1971) 230.
[17] F.J. Farrel, V.A. Maroni, T.G. Spiro, Inorg. Chem. 8 (1969) 2638.
[18] C. Rocchiccioli-Deltcheff, R. Thouvenot, M. Fouassier, Inorg. Chem. 21 (1982) 30.
[19] C. Rocchiccioli-Deltcheff, M. Fournier, R. Franck, R. Thouvenot, J. Mol. Struct. 114 (1984) 49.
[20] M.-M. Rohmer, R. Ernenwein, M. Ulmschneider, R. Wiest, M. Bénard, Int. J. Quantum. Chem. 40 (1991) 723.
[21] J.-Y. Kempf, M.-M. Rohmer, J.-M. Poblet, C. Bo, M. Bérnard, J. Am. Chem. Soc. 114 (1992) 1136.

[22] M.-M. Rohmer, M. Bérnard, J. Am. Chem. Soc. 116 (1994) 6959.
[23] J. Devémy, M.-M. Rohmer, M. Bérnard, R. Ernenwein, Int. J. Quantum Chem. 58 (1996) 267.
[24] M.-M. Rohmer, J. Devémy, R. Wiest, M. Bérnard, J. Am. Chem. Soc. 118 (1996) 13007.
[25] J.M. Maestre, J.P. Sarasa, C. Bo, J.M. Poblet, Inorg. Chem. 37 (1998) 3071.
[26] J.M. Maestre, J.M. Poblet, C. Bo, N. Casañ-Pastor, P. Gomez-Romero, Inorg. Chem. 37 (1998) 3444.
[27] A. Dolbecq, A. Guirauden, M. Fourmigué, K. Boubekeur, P. Batail, M.-M. Rohmer, M. Bérnard, C. Coulon, M. Sallé, P. Blanchard, J. Chem. Soc., Dalton Trans. (1999) 1241.
[28] J.M. Maestre, X. López, C. Bo, J.M. Poblet, N. Casañ-Pastor, J. Am. Chem. Soc. 123 (2001) 3749.
[29] M.-M. Rohmer, M. Bérnard, J.-P. Blaudeau, J.M. Maestre, J.M. Poblet, Coord. Chem. Rev. 178–180 (1998) 1019.
[30] X. López, J.M. Maestre, J.M. Poblet, C. Bo, J. Am. Chem. Soc. 123 (2001) 9571.
[31] A.J. Bridgeman, G. Cavigliasso, Polyhedron 20 (2001) 2269.
[32] A.J. Bridgeman, G. Cavigliasso, J. Phys. Chem. A 105 (2001) 7111.
[33] A.J. Bridgeman, G. Cavigliasso, Polyhedron 20 (2001) 3101.
[34] A.J. Bridgeman, G. Cavigliasso, J. Chem. Soc. Dalton Trans. (2001) 3556.
[35] A.J. Bridgeman, G. Cavigliasso, Inorg. Chem. 41 (2002) 1761.
[36] H. Duclusaud, S.A. Borshch, Inorg. Chem. 38 (1999) 3489.
[37] H. Duclusaud, S.A. Borshch, J. Am. Chem. Soc. 123 (2001) 2835.
[38] S.A. Borshch, H. Duclusaud, J.M.M. Millet, Appl. Catal. A 200 (2000) 103.
[39] ADF2000.02 E.J. Baerends, D.E. Ellis, P. Ros, Chem. Phys. 2 (1973) 41;
L. Versluis, T. Ziegler, J. Chem. Phys. 322 (1988) 88;
G. te Velde, E.J. Baerends, J. Comput. Phys. 99 (1992) 84;
C. Fonseca Guerra, J.G. Snijders, G. te Velde, E.J. Baerends, Theor. Chem. Acc. 99 (1998) 391.
[40] G. te Velde, F.M. Bickelhaupt, E.J. Baerends, G. Fonseca Guerra, J.C. Snijders, T. Ziegler, J. Comput. Chem. 22 (2001) 931.
[41] M.J. Frisch et al., GAUSSIAN 98, Revision A.3, Gaussian Inc., Pittsburgh, PA, 1998.
[42] M. Torrent, P. Gili, M. Duran, M. Sola, J. Chem. Phys. 104 (1996) 9499.
[43] M. Torrent, P. Gili, M. Duran, M. Sola, Int. J. Quantum Chem. 61 (1997) 405.
[44] S.H. Vosko, L. Wilk, M. Nusair, Can. J. Phys. 58 (1980) 1200.
[45] A.D. Becke, Phys. Rev. A 38 (1988) 3098.
[46] J.P. Perdew, Phys. Rev. B 33 (1986) 8822.
[47] C. Lee, W. Yang, R.G. Parr, Phys. Rev. B 37 (1988) 785.
[48] A.D. Becke, J. Chem. Phys. 104 (1996) 1040.
[49] G. Herzberg, Molecular Spectra and Molecular Structure II. Infrared and Raman Spectra of Polyatomic Molecules, D. Van Nostrand, New York, 1964.
[50] J.E. McGrady, R. Stranger, T. Lovell, J. Phys. Chem. A 101 (1997) 6265.
[51] A.C. Stückl, C.A. Daul, H.U. Güdel, J. Chem. Phys. 107 (1997) 4606.
[52] W. Koch, M.X. Holthausen, A Chemist's Guide to Density Functional Theory, second ed., Wiley-VCH, Weinheim, 2001.